JOURNAL OF COMPUTATIONAL PHYSICS **138,** 501–519 (1997)
ARTICLE NO. CP975829

A Boundary Element Method for Multiple Moving Boundary Problems

M. Zerroukat* and L. C. Wrobel†

*Wessex Institute of Technology, Ashurst Lodge, Ashurst, Hampshire SO40 7AA, United Kingdom; and †Department of Mechanical Engineering, Brunel University, Uxbridge UB8 3PH, United Kingdom

Received February 13, 1996; revised July 31, 1997

A boundary element formulation for the solution of multiple moving boundary problems is presented and tested herein. A heat transfer problem involving heating of solid, melting of solid, and partial vaporisation of liquid is considered. Numerical results show that the boundary element method is more suitable and more accurate than both finite difference and finite element methods for this kind of problem.

Key Words: Stefan problems; phase change; moving boundaries; boundary element method.

1. INTRODUCTION

Many physical and engineering processes can be modelled as moving boundary, or Stefan, problems, where a set of partial differential equations is to be solved for a domain whose boundaries are not known *a priori* but have to be determined as an integral part of the solution. Due to the complexity of the boundary conditions, analytical solutions are impossible to obtain, with the exception of relatively simple cases, and therefore, recourse is often made to numerical techniques, such as Finite Difference (FD), Finite Element (FE), and Boundary Element (BE) methods. Most numerical methods developed for such problems are conceived for a single moving boundary separating two adjacent domains [1].

Since one-moving boundary problems have a wide range of application in physics and engineering, they became synonymous with Stefan problems. However, many other processes, in which several boundaries separating different regions are simultaneously in motion, also fall in that category. A heat transfer process involving melting of solid and partial vaporisation of the liquid is one of such problems. Multi-moving boundary problems have been dealt with by both FD and FE methods.

0021-9991/97 $25.00

Zerroukat and Chatwin [2] used an explicit exponential finite-difference solution for the heat equation coupled with a variable mesh, according to the velocity of the moving boundary. Bonnerot and Jamet [3] extended the adaptive space-time finite element scheme reported in [4] to deal with multi-phase problems. They used curved triangular elements for appearing boundaries and curved trapezoidal elements elsewhere. An attractive feature of this method, especially for moving boundaries, lies in the fact that the space discretization at any time step can be completely independent from that of the previous step.

In recent years, the boundary element method has emerged as a powerful and cost effective alternative to FD and FE methods, for many problems particularly those with variable and extended domains, since only the discretization of the boundary is necessary [5]. In this paper a boundary element based technique, capable of dealing with multi-moving boundaries with great ease, is presented and tested on a heat transfer problem involving appearing and disappearing phases with several simultaneous moving boundaries. For comparison purposes the collapse of a solid wall treated in references [2, 3] is also considered.

2. BOUNDARY INTEGRAL FORMULATION

Consider the general heat equation

$$C\frac{\partial T(\mathbf{x}, t)}{\partial t} = K\nabla^2 T(\mathbf{x}, t) \qquad \text{for } \mathbf{x} \in \Omega(t) \subset \mathbb{R}^d, t > 0 \tag{1}$$

with certain conditions on the boundary $\Gamma = \partial\Omega$. $T(\mathbf{x}, t)$, C, and K denote the temperature at the spatial position $\mathbf{x}$ at time t, heat capacity per unit volume, and heat conductivity, respectively. The integral equation corresponding to (1) over the entire space-time domain can be obtained by starting with the weighted residual statement

$$\int_{t_0}^{\tau} dt \int_{\Omega(t)} G\left(\alpha\nabla^2 T - \frac{\partial T}{\partial t}\right) d\Omega = 0, \tag{2}$$

where $\alpha = K/C$ denotes thermal diffusivity and G is the free space Green's function given by

$$G(\boldsymbol{\xi}, \mathbf{x}, \tau, t) = \frac{1}{[4\pi\alpha(\tau - t)]^{d/2}} \exp\left\{-\frac{r^2}{4\alpha(\tau - t)}\right\} \tag{3}$$

which is the solution of

$$\frac{\partial G}{\partial t} + \alpha\nabla^2 G = -\delta(\boldsymbol{\xi} - \mathbf{x})\delta(\tau - t), \tag{4}$$

where δ denotes the Dirac delta function, d is the dimension of the problem, and r is the Euclidian distance between the field point $\mathbf{x}$ and the source point $\boldsymbol{\xi}$. Using Green's second identity and making use of the Reynolds transport theorem, which can also be seen as the Leibnitz rule for a deformable domain, the integral representation is obtained in the form [6–13]

$$c(\boldsymbol{\xi})T(\boldsymbol{\xi},\tau) = \alpha\int_{t_0}^{\tau} dt \int_{\Gamma(t)} \left[G\frac{\partial T}{\partial n} - T\frac{\partial G}{\partial n} + \frac{1}{\alpha} TG(\vec{n}\cdot\vec{v}) \right] d\Gamma + \int_{\Omega(t_0)} GT\, d\Omega, \quad (5)$$

where $(\vec{n}\cdot\vec{v})$ is the rate of the boundary motion in the outward normal direction and $c(\boldsymbol{\xi})$ is a constant which depends on the position of the source point $\boldsymbol{\xi}$, the smoothness and shape of the boundary,

$$c(\boldsymbol{\xi}) = \begin{cases} 0 & \text{for } \boldsymbol{\xi} \notin \Omega \\ 1 & \text{for } \boldsymbol{\xi} \in \Omega \\ \beta/2\pi & \text{for } \boldsymbol{\xi} \in \Gamma, \end{cases} \quad (6)$$

where β is a function of the local geometry of the boundary at the source point $\boldsymbol{\xi}$. For a smooth boundary $\beta = \pi$.

3. APPLICATION TO MULTIPLE MOVING BOUNDARIES

Consider a heat transfer problem in which a material slab of thickness a, initially at constant temperature T_0, is subjected to two different heat fluxes $F_1(t)$ and $F_2(t)$ at $x = 0$ and $x = a$, respectively (see Fig. 1). After some time the temperature, at $x = 0$ or $x = a$, reaches the melting point T_m and a moving boundary separating liquid from solid appears. Another vapour/liquid interface appears when the temperature reaches T_v. Assuming that the vapour, or removed material, is removed as soon as it appeared, the problem is to track the position of the different moving boundaries simultaneously in motion. The problem can be written as

$$\frac{\partial T}{\partial t} = \alpha_j \frac{\partial^2 T}{\partial x^2}, \qquad (x,t) \in R_j, j = 1,2,3, \quad (7)$$

where $\alpha_1 = \alpha_3 = \alpha_l$ and $\alpha_2 = \alpha_s$; subscripts l and s refer to liquid and solid, respectively. The initial and boundary conditions are

$$T(x,0) = T_0 \quad (8)$$

$$-K_2 \frac{\partial T}{\partial x}\bigg|_{x=0} = F_1(t); \qquad \tau_0 < t < \tau_2; \qquad K_2 \frac{\partial T}{\partial x}\bigg|_{x=a} = F_2(t), \qquad \tau_0 < t < \tau_3 \quad (9)$$

$$-K_1 \frac{\partial T}{\partial x}\bigg|_{x=0} = F_1(t); \qquad \tau_2 < t < \tau_1; \qquad K_1 \frac{\partial T}{\partial x}\bigg|_{x=a} = F_2(t), \qquad \tau_3 < t < \tau_4 \quad (10)$$

$$T(X_2,t) = T(X_3,t) = T_m; \qquad T(X_1,t) = T(X_4,t) = T_v \quad (11)$$

$$(-1)^j \lambda_m \frac{dX_j}{dt} = K_j \frac{\partial T}{\partial x}\bigg|_{X_j^+} - K_{j-1} \frac{\partial T}{\partial x}\bigg|_{X_j^-} \qquad \text{for } j = 2,3 \quad (12)$$

$$\lambda_v \frac{dX_j}{dt} = K_l \frac{\partial T}{\partial x}\bigg|_{X_j} + (-1)^{j+1} F_{\min(j,2)}(t), \qquad j = 1,4, \quad (13)$$

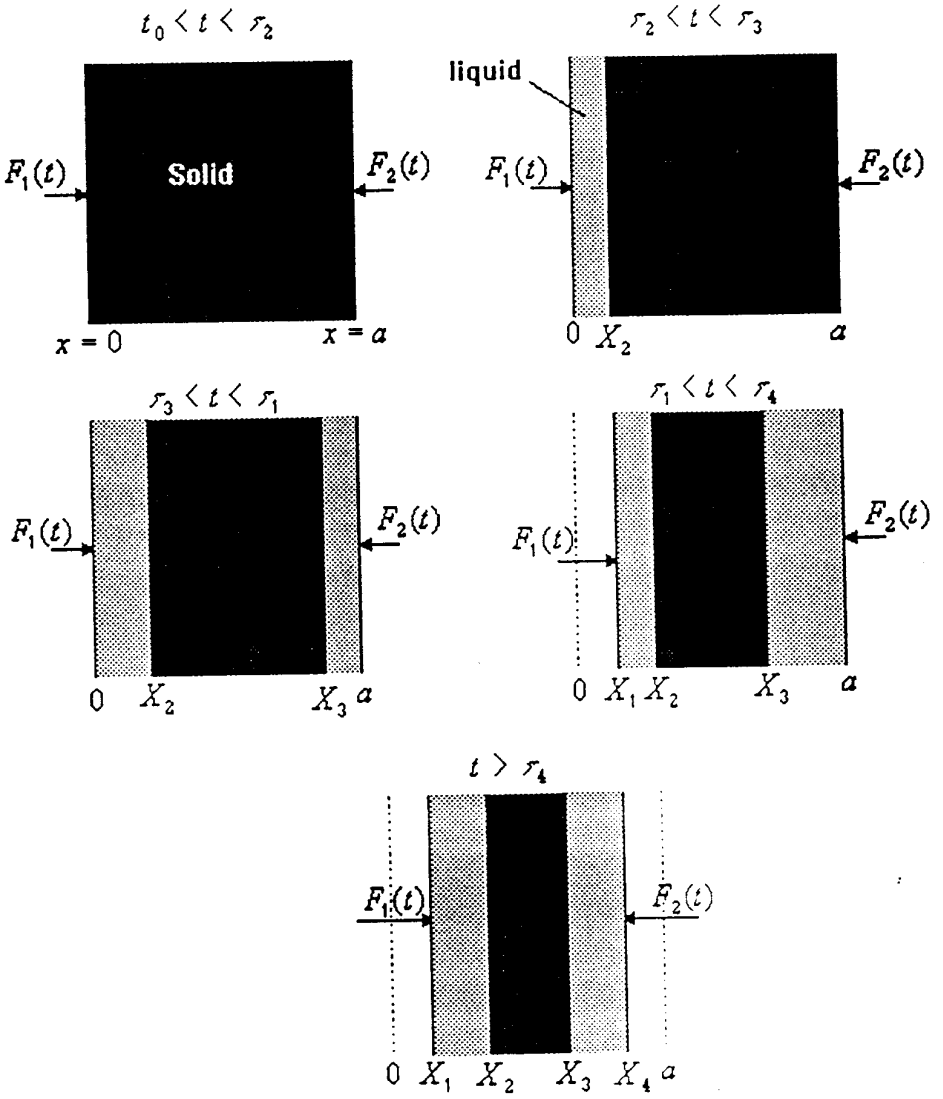

FIG. 1. Different stages of the process.

where τ_j is the time of appearance of the moving boundary $X_j(t)$ (see Fig. 2); λ_m, λ_v are latent heat of melting per unit volume and latent heat of vaporisation per unit volume, respectively.

Applying Eq. (5) to any region Ω_j, $j = 1 \ldots 3$, bounded by the moving boundaries X_j and X_{j+1}, the following can be written,

$$c(\xi)T_j(\xi, t_n) = \alpha_j \int_{t_0}^{t_n} \left[G(\xi, x, t_n, t) \frac{\partial T(x,t)}{\partial x} - T(x,t) \frac{\partial G(\xi, x, t_n, t)}{\partial x} \right.$$

$$\left. + \frac{1}{\alpha_j} T(x,t) G(\xi, x, t_n, t) \frac{dx}{dt} \right]_{X_j(t)}^{X_{j+1}(t)} dt + \psi_j(\xi, t_n), \tag{14}$$

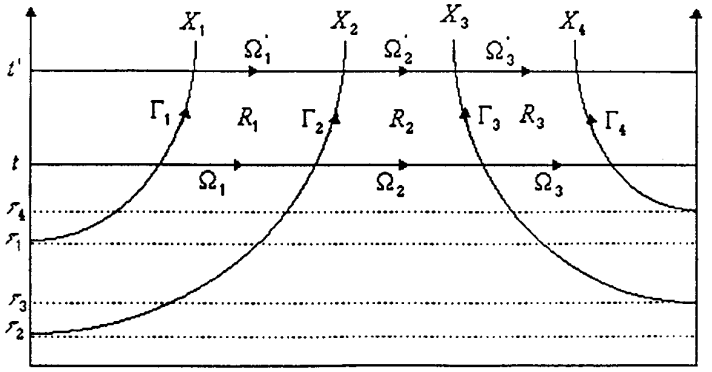

FIG. 2. Adjacent domains R_j with their separating boundaries X_j.

where

$$\psi_2(\xi, t_n) = \int_0^a T(x, t_0) G(\xi, x, t_n, t_0)\, dx; \qquad \psi_1(\xi, t_n) = \psi_3(\xi, t_n) = 0. \tag{15}$$

Applying Eq. (14) to each extreme point of the domain Ω_j and assuming a stepwise variation of temperature and its derivatives, and a linear propagation of the moving boundary $X_j^i = X_j^{i-1} + \overline{X}_j^i(t_i - t_{i-1})$, within each time step, the following system for the time step t_n is obtained,

$$\begin{aligned}\frac{1}{2} u_j^n = \alpha_j \sum_{i=i_{j+1}}^{n} \Bigg\{ & g(X_j, X_{j+1}, t_n, t_i) \left(q_{j+1}^{i-} + \frac{1}{\alpha_j} \overline{X}_{j+1}^i u_{j+1}^i \right) \\ & - u_{j+1}^i h(X_j, X_{j+1}, t_n, t_i) \Bigg\} - \alpha_j \sum_{i=i_j}^{n} \Bigg\{ g(X_j, X_j, t_n, t_i) \\ & \left(q_j^{i+} + \frac{1}{\alpha_j} \overline{X}_j^i u_j^i \right) - u_j^i h(X_j, X_j, t_n, t_i) \Bigg\} + \psi_j(X_j, t_n) \end{aligned} \tag{16}$$

$$\begin{aligned}\frac{1}{2} u_{j+1}^n = \alpha_j \sum_{i=i_{j+1}}^{n} \Bigg\{ & g(X_{j+1}, X_{j+1}, t_n, t_i) \left(q_{j+1}^{i-} + \frac{1}{\alpha_j} \overline{X}_{j+1}^i u_{j+1}^i \right) \\ & - u_{j+1}^i h(X_{j+1}, X_{j+1}, t_n, t_i) \Bigg\} - \alpha_j \sum_{i=i_j}^{n} \Bigg\{ g(X_{j+1}, X_j, t_n, t_i) \\ & \left(q_j^{i+} + \frac{1}{\alpha_j} \overline{X}_j^i u_j^i \right) - u_j^i h(X_{j+1}, X_j, t_n, t_i) \Bigg\} + \psi_j(X_{j+1}, t_n), \end{aligned} \tag{17}$$

where $u_j^n = T(X_j, t_n)$, $q_j^{n+} = (\partial T/\partial x)(X_j^+, t_n)$, $q_j^{n-} = (\partial T/\partial x)(X_j^-, t_n)$, $\overline{X}_j^i = (\partial X_j/\partial t)_{t_i}$, $X_j^i = X_j(t_i)$, i_j is the time index of appearance of X_j, and

$$g(\xi, X, \tau, t_i) = \int_{t_{i-1}}^{t_i} G(\xi, X(t), \tau, t)\, dt, \qquad h(\xi, X, \tau, t_i) = \int_{t_{i-1}}^{t_i} \frac{\partial G(\xi, X(t), \tau, t)}{\partial x}\, dt. \tag{18}$$

The integrals in (18) can be calculated analytically; see Appendix for details. After some manipulation and using a matrix form, for each region Ω_j a system of equations must be solved

$$\mathbf{G}_j^n \begin{Bmatrix} u_j^n \\ u_{j+1}^n \end{Bmatrix} + \mathbf{H}_j^n \begin{Bmatrix} q_j^{n+} \\ q_{j+1}^{n-} \end{Bmatrix} = \mathbf{M}_j^n, \tag{19}$$

where $\mathbf{G}_j^n$ and $\mathbf{H}_j^n$ are matrices of 2×2 elements (see details in Appendix).

It can be seen that to solve the system (19), $\overline{X}_j^n$ and X_j^n must be known. Since the velocity and the position of the moving boundaries are not known in advance, an iterative procedure is employed. Assumed velocities and positions of the moving boundaries, using an extrapolation from the two previous time steps, are used to solve (19). The velocities are then updated using the solution of (19) and the Stefan conditions at the moving boundaries. This process is repeated until a desired accuracy is achieved. In general, for an arbitrary number $(J-1)$ of adjacent domains separated by J moving boundaries, the following system with $2(J-1)$ unknowns, due to the necessity of calculating the heat flux on both sides of the interface, must be solved,

$$\mathbf{G}_n^k \begin{Bmatrix} u_1^n \\ u_2^n \\ u_2^n \\ \vdots \\ u_j^n \\ u_j^n \\ u_{j+1}^n \\ \vdots \\ u_{J-1}^n \\ u_{J-1}^n \\ u_J^n \end{Bmatrix}^k + \mathbf{H}_n^k \begin{Bmatrix} q_1^{n+} \\ q_2^{n-} \\ q_2^{n+} \\ \vdots \\ q_j^{n-} \\ q_j^{n+} \\ q_{j+1}^{n-} \\ \vdots \\ q_{J-1}^{n-} \\ q_{J-1}^{n+} \\ q_J^{n-} \end{Bmatrix}^k = \mathbf{M}_n^k, \tag{20}$$

where $\mathbf{G}_n^k$, $\mathbf{H}_n^k$ are tri-diagonal matrices and $\mathbf{M}_n^k$ a vector computed for each iteration k for each time step n.

If the Stefan conditions (12) and (13) are rewritten as,

$$\overline{X}_j = \varphi(q_j^-, q_j^+, F_1, F_2, \lambda_m, \lambda_v) \tag{21}$$

the velocity $(\overline{X}_j^n)^k$ at the kth iteration is given by

$$(\overline{X}_j^n)^k = (1-\omega_j)(\overline{X}_j^n)^{k-1} + \omega_j(\varphi_j^n)^{k-1}, \tag{22}$$

where ω_j is a relaxation factor $(0 < \omega_j \leq 1)$ and,

$$(\varphi_j^n)^k = \varphi((q_j^n)_{X_j^-}^k, (q_j^n)_{X_j^+}^k, F_1^n, F_2^n, \lambda_m, \lambda_v). \tag{23}$$

It seems quite instinctive to take $\omega_j = 1$; however, numerical experiments show that the scheme may converge for certain time steps but not for others. The choice of ω_j must be varied in order to get satisfactory convergence for all the time steps and for different situations. Generally a choice of $0.4 \leq \omega_j \leq 0.6$ is very satisfactory when φ is a function of two or more temperature gradients; however, a choice $0.8 \leq \omega_j \leq 1.0$ is more suitable for the case of φ as function of one temperature derivative, like in one-phase problems. The iterative process is stopped when

$$\max\left(\left|100 \times \frac{(\overline{X}_j^n)^{k+1} - (\overline{X}_j^n)^k}{(\overline{X}_j^n)^k}\right|, j = 1, J\right) \leq \varepsilon, \tag{24}$$

where ε is a small prescribed relative error. It is worth mentioning that, for a multi-dimensional moving boundary problem, the above iteration scheme would possibly need to be replaced by more globally convergent schemes such as quasi-Newton or Fletcher–Powell minimization algorithms [14]. However, for the present problem, the relaxation scheme has been shown to be satisfactory with an average number of only two iterations per step.

It has been noticed that the changes in $\mathbf{M}_n^k$, in Eq. (20), are small from one iteration to another (i.e., $\mathbf{M}_n^k = \mathbf{M}_n^{k-1} + O(\Delta t^3)$; see Table IV). Therefore, the vector $\mathbf{M}_n^k$, which involves all the previous time steps, can be calculated only once, for each time step n, using the velocities and positions of the moving boundaries for the first iteration only ($k = 1$); i.e., it is CPU-cost effective to solve, instead of (20), the following system (omitting the subscript n):

$$\mathbf{G}^k\mathbf{u}^k + \mathbf{H}^k\mathbf{q}^k = \mathbf{M}^1. \tag{25}$$

Since at each boundary either the heat fluxes or the temperature are to be determined, but not both, the system of equations (20) or (25) can be transformed as $\mathbf{Ax} = \mathbf{b}$ with $2(J - 1)$ unknowns, and solved using a standard Gauss elimination technique.

In order to validate the numerical results, an energy balance check is performed at each time step. Multiplying (1) by a continuous function ϕ and integrating by parts gives

$$-\iint_R CT\frac{\partial\phi}{\partial t}\,dx\,dt + \iint_R K\frac{\partial\phi}{\partial x}\frac{\partial T}{\partial x}\,dx\,dt - \int_{\partial R}\phi\left(CT\,dx + K\frac{\partial T}{\partial x}\,dt\right) = 0, \tag{26}$$

where $R \subset [0, a] \times [0, t_e]$ and t_e denotes the time at which the process ends. For the particular case of $\phi = 1$ the following energy balance expression is obtained

$$\int_{\partial R}\left(CT\,dx + K\frac{\partial T}{\partial x}\,dt\right) = 0. \tag{27}$$

Applying Eq. (27) to the different regions $R_j = [X_j, X_{j+1}] \times [t, t']$, $j = 1, 3$ (see Fig. 2) and making use of the Stefan conditions (12) and (13), we obtain

$$\sum_{j=1}^{3} C_j \left[\int_{\Omega_j'} T dx - \int_{\Omega_j} T dx + \int_{\Gamma_j} T dx - \int_{\Gamma_{j+1}} T dx \right] + \lambda_v \Delta X_1 - \int_t^{t'} F_1(t)\, dt + \lambda_m \Delta X_2 - \lambda_m \Delta X_3 - \lambda_v \Delta X_4 - \int_t^{t'} F_2(t)\, dt = 0, \tag{28}$$

where $\Delta X_j = X_j(t') - X_j(t)$. The left-hand side of (28) can be subdivided into

$$E_1 = C_l \left[\int_{\Omega_1'} T dx - \int_{\Omega_1} T dx + \int_{\Omega_3'} T dx - \int_{\Omega_3} T dx - T_m(\Delta X_2 - \Delta X_3) - T_v(\Delta X_4 - \Delta X_1) \right] \tag{29}$$

$$E_2 = C_s \left[\int_{\Omega_2'} T dx - \int_{\Omega_2} T dx - T_m(\Delta X_3 - \Delta X_2) \right] \tag{30}$$

$$E_3 = \lambda_m(\Delta X_2 - \Delta X_3) \tag{31}$$

$$E_4 = \lambda_v(\Delta X_1 - \Delta X_4) \tag{32}$$

$$E_5 = \int_t^{t'} [F_2(t) + F_1(t)]\, dt. \tag{33}$$

Equation (28) can also be written as

$$E_5 - \sum_{i=1}^{4} E_i = 0. \tag{34}$$

The quantities in (29) to (33) can be interpreted physically as:

E_1: Energy to heat the liquid regions R_1 and R_3.

E_2: Energy to heat the solid region R_2.

E_3: Energy to melt the solid.

E_4: Energy to vaporise the liquid.

E_5: Energy provided.

4. RESULTS AND DISCUSSION

The method described in the previous section is used to solve the problem defined by Eqs. (7) to (13) with the following example of data, which will be referred to as *problem 1:*

$$a = 2.0\ \text{m},\ T(x, 0) = 20\ ^\circ\text{C},\ C_l = 3.5\ \text{W/m}^3\ ^\circ\text{C},$$
$$C_s = 4.0\ \text{W/m}^3\ ^\circ\text{C},\ K_l = 0.30\ \text{W/m}^\circ\text{C},\ K_s = 0.25\ \text{W/m}^\circ\text{C},$$
$$\lambda_m = 2000\ \text{J/m}^3,\ \lambda_v = 30000\ \text{J/m}^3,\ T_m = 600\ ^\circ\text{C},\ T_v = 2000\ ^\circ\text{C},$$
$$F_1(t) = b_0 + b_1 t + b_2 t^2 + b_3 t^3\ \text{W/m}^2,\ F_2(t) = c_0 + c_1 t + c_2 t^2 + c_3 t^3\ \text{W/m}^2.$$

TABLE I

Velocity and Position of the Moving Boundaries for Problem 1, with the Corresponding Relative Error Due to the Energy Balance, ε_e, also tabulated; $\Delta t = 1/20$, $b = \{30, 5, 0, 10\}$, and $c = \{15, 20, 15, 0\}$

Time [s]	Velocities [m/s]				Positions [m]				Error [%]
t	$\overline{X}_1(t)$	$\overline{X}_2(t)$	$\overline{X}_3(t)$	$\overline{X}_4(t)$	$X_1(t)$	$X_2(t)$	$X_3(t)$	$X_4(t)$	$\epsilon_e(t)$
3.6478	–	–	–	–	–	–	–	–	0.63266
3.7500	–	0.06561	–	–	–	0.00547	–	–	0.50622
4.0000	–	0.12521	–	–	–	0.03174	–	–	0.35917
4.8000	–	0.18700	−0.06290	–	–	0.16455	1.98723	–	0.46619
5.8000	0.01909	0.19784	−0.11721	–	0.00237	0.36172	1.88970	–	0.35467
6.2000	0.04079	0.16552	−0.12673	–	0.01511	0.43320	1.84047	–	0.03608
7.0000	0.07949	0.13962	−0.13906	–	0.06408	0.55208	1.72258	–	0.02130
7.8000	0.12249	0.13891	−0.15095	–	0.14554	0.66231	1.61747	–	0.02265
8.9000	0.19330	0.16640	−0.17143	−0.01460	0.31958	0.82761	1.43879	1.99576	0.05510
9.1000	0.20784	0.17572	−0.17204	−0.01821	0.36005	0.86203	1.40443	1.99238	0.03307
9.3000	0.22294	0.18646	−0.17303	−0.02146	0.40350	0.89850	1.36992	1.98832	0.02507
9.5000	0.23860	0.19811	−0.17456	−0.02450	0.45003	0.93723	1.33512	1.98365	0.02731
9.8000	0.26321	0.21460	−0.17562	−0.02884	0.52588	0.99964	1.28248	1.97553	0.01560
10.100	0.28919	0.22469	−0.16982	−0.03303	0.60936	1.06599	1.23059	1.96614	0.01427
10.300	0.30724	0.22933	−0.16285	−0.03577	0.66944	1.11148	1.19749	1.95919	0.01387
10.400	0.31648	0.23241	−0.15949	−0.03713	0.70086	1.13464	1.18146	1.95552	0.01358
10.519	0.33054	0.23806	−0.15507	−0.03915	0.73959	1.16275	1.16275	1.95095	0.01247
10.700	0.34533	–	–	−0.04085	0.80047	–	–	1.94394	0.01356
10.900	0.37116	–	–	−0.04381	0.87270	–	–	1.93539	0.01176
11.100	0.39971	–	–	−0.04687	0.95046	–	–	1.92626	0.00965
11.300	0.42990	–	–	−0.05035	1.03415	–	–	1.91645	0.00945
11.450	0.45375	–	–	−0.05328	1.10102	–	–	1.90861	0.00850

Note. $\varepsilon_e(t) = |100 \times (E_5(t) - \sum_{i=1}^{4} E_i(t))/E_5(t)|$, similar to Eq. (34), where $E_i(t)$ is the energy calculated using (29) to (33) with Ω_i the domain of region i at the time $t - \Delta t$, and Ω_i' the domain at time t. $E_5(t) = \int_{t-\Delta t}^{t} \{F_1(\tau) + F_2(\tau)\}\, d\tau$.

Table I shows the positions and velocities of the different moving boundaries at certain times, with $\Delta t = 1/20$ s, $\omega_2 = \omega_3 = 0.45$, $\omega_1 = \omega_4 = 1.0$, $b = \{30, 5, 0, 10\}$, $c = \{15, 20, 15, 0\}$, and $\varepsilon = 0.05$ percent. In order to validate the numerical results, the energy balance (34) is checked at each time step, by evaluating the relative error ϵ_e, between the energy provided and consumed. For that end, the temperature at several internal points is computed to calculate the integrals in Eqs. (29) and (30); however, these calculations are a post-processing task and are not involved in the solution of the problem (i.e., positions of and heat fluxes at the moving boundaries). It can be seen, from Table I, that the numerical results agree with the energy balance where ϵ_e is relatively small. Furthermore, ϵ_e contains another error due to evaluations of integrals (29) and (30), which can be reduced by increasing the number of internal points. This integration error is higher when the temperature gradient is sharp, but decreases when the gradient is diminished; this is clearly illustrated in Table I where ϵ_e decreases with time.

Figures 3 and 4 show the velocity history of the melting and vaporisation fronts for *problem 1* when the boundaries are subjected to different heat fluxes. The corresponding moving boundary positions are shown in Fig. 5. Figure 3 shows that when the two heat flux inputs are of similar order, the two melting interfaces behave in a similar manner. There is only a time delay and a difference in the direction of propagation between the two. This is also valid for the two vaporisation fronts. In general, the Liquid/Solid (L/S) interface accelerates sharply just after its appearance, then its velocity starts to decrease due to the increase of thermal-resistance

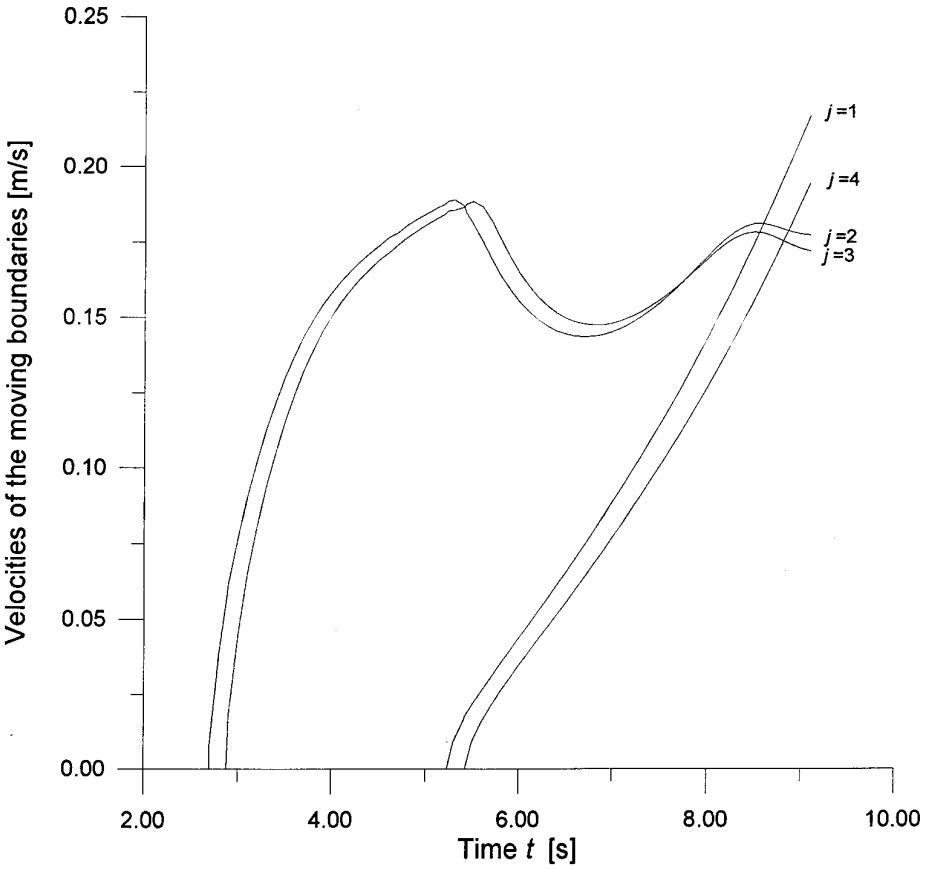

FIG. 3. Velocities $|\overline{X}_j|$ versus time for *problem 1* when $b = \{200, 10, 0, 10\}$ and $c = \{180, 10, 0, 9\}$.

of the liquid as the thickness of the melting region increases. It reaches a maximum speed just before the appearance of the vaporisation front. When the Vapour/Liquid (V/L) interface appears, the melting boundary slows sharply because of the loss of heat due to vaporisation. The V/L accelerates in the initial instance, and then continues to accelerate at rates proportional to the heat flux input throughout the process. The L/S velocity reaches a minimum after the appearance of the V/L, then it starts to increase again. This is due to the fact that the heat flux entering the solid region decreases as the melting fronts approach each other (i.e., there is less energy absorbed as the whole solid region approaches the melting point). The heat flux at the L/S decreases with a smaller gradient than the heat entering the solid, resulting in greater proportion of energy being available to melt the solid material. Just before the total melting, the L/S velocity starts to decrease again due to the decreasing heat flux throughout the liquid region and the almost negligible heat flux exiting the region.

Figure 4 shows the histories of the velocities when the two extremities are subjected to heat fluxes of different orders. The melting front which starts from the extremity where a quadratic heat flux is prescribed behaves more or less in a manner

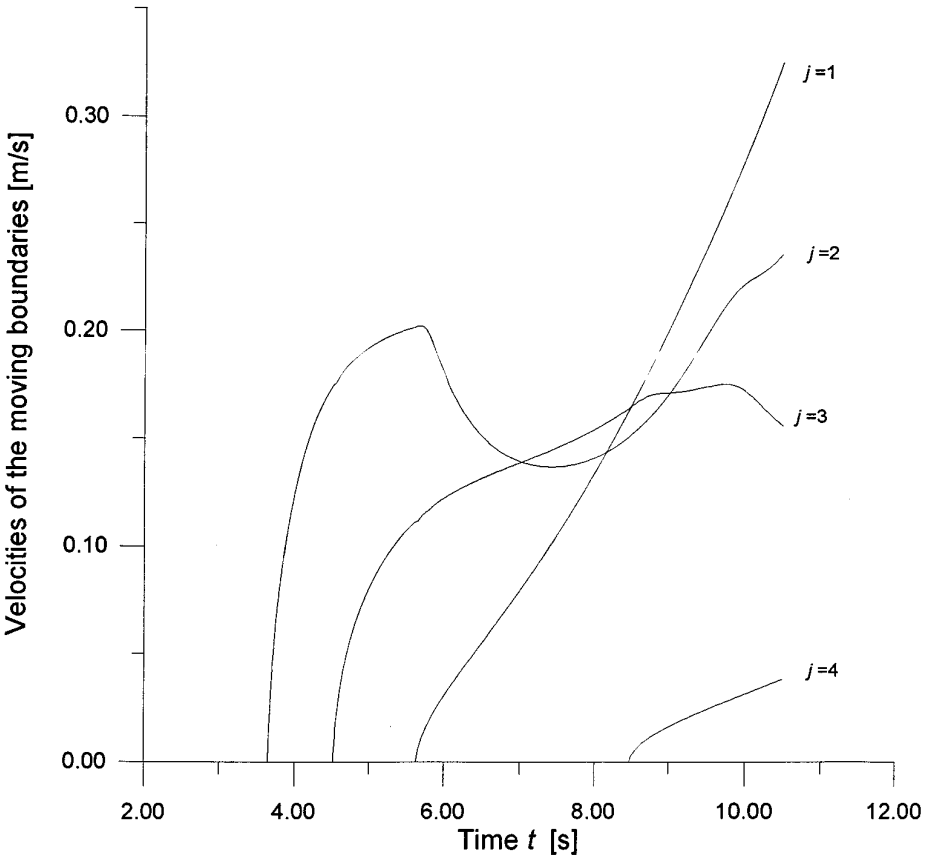

FIG. 4. Velocities $|\overline{X}_j|$ versus time for *problem 1* when $b = \{30, 5, 0, 10\}$ and $c = \{15, 20, 15, 0\}$.

similar to that shown in Fig. 3. Although the second melting interface shows a similar pattern, the larger delay prevented the second boundary to have a similar curve. For instance, the concavity between the two maxima is almost flat.

Table II shows that the order of convergence *in time* of the method is one. This is not established mathematically but verified numerically. Furthermore, it must be emphasised that this analysis only concerns time since there is no space discretization. The numerical procedure used for determining the order of convergence is similar to that described in [4].

Let $z = z(u)$ be a certain functional of the solution u. For example, u in Table II is taken as $T(a, t_c)$, $X_2(t_c)$, and $X_3(t_c)$, respectively; t_c being an arbitrary given time ($t_c = 5.0$ in Table II). Let $\tilde{z}_i$ be the approximate value of z for a given Δt_i. We want to determine a positive number p such that

$$\tilde{z}_i - z \simeq c\,(\Delta t_i)^p, \tag{35}$$

where c is a constant. Let Δt_{i-2}, Δt_{i-1}, and Δt_i be three successive values of Δt with $\Delta t_{i-2} < \Delta t_{i-1} < \Delta t_i$. If (35) holds, then

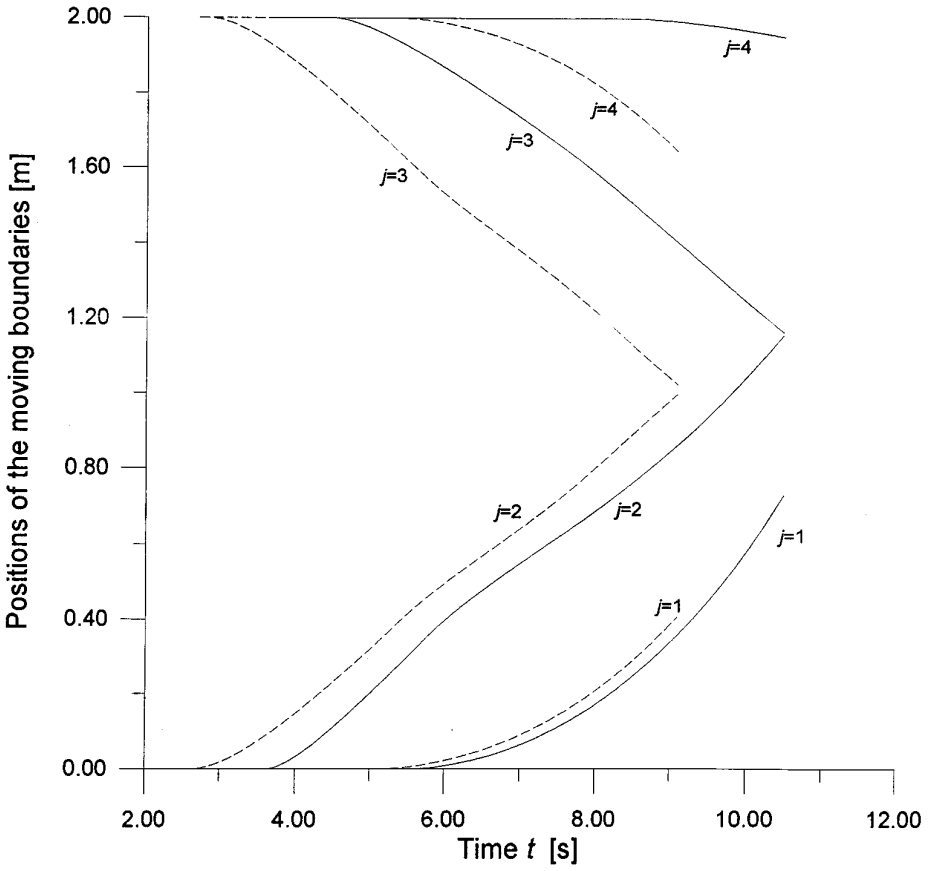

FIG. 5. Positions of the moving boundaries (X_j) versus time for *problem 1*. Solid lines are for $b = \{30, 5, 0, 10\}$, $c = \{15, 20, 15, 0\}$ and dashed lines are for $b = \{200, 10, 0, 10\}$ and $c = \{180, 10, 0, 9\}$.

$$\phi(\tilde{z}_i) = \frac{\tilde{z}_i - \tilde{z}_{i-2}}{\tilde{z}_{i-1} - \tilde{z}_{i-2}} \simeq \frac{(\Delta t_i)^p - (\Delta t_{i-2})^p}{(\Delta t_{i-1})^p - (\Delta t_{i-2})^p} = \frac{r_2^p - 1}{r_1^p - 1} = f(p), \tag{36}$$

where $r_2 = \Delta t_i / \Delta t_{i-2}$ and $r_1 = \Delta t_{i-1} / \Delta t_{i-2}$. Since $f(p)$ increases monotonically and $f(p) > f(0) = (\log r_2 / \log r_1)$, one can determine a unique $p = p(\Delta t_i, \Delta t_{i-1}, \Delta t_{i-2})$

TABLE II
Convergence of $\tilde{z}$ for Different Time Steps Δt

Δt	$\tilde{z} = T(a, t_c)$	p	$\tilde{z} = X_2(t_c)$	p	$\tilde{z} = X_3(t_c)$	p
1/6	651.1960	–	0.2169592	–	1.967344	–
1/18	644.2786	–	0.2033089	–	1.972097	–
1/30	642.9516	1.05	0.2005078	0.97	1.973044	1.00
1/64	641.8986	1.01	0.1981973	0.95	1.973827	0.94
1/100	641.5837	1.09	0.1974600	0.99	1.974077	0.99
1/200	641.3195	1.11	0.1968036	1.00	1.974304	0.97

TABLE III
Comparison of t_m, t_v, t_e, and $V(t_e)$ for Different Time Steps Δt

Δt [s]	t_m [s]	t_v [s]	t_e [s]	$V(t_e)$ [m]
FD method [2]				
1/4	0.32740	1.58887	9.15907	0.26318
1/8	0.32660	1.58783	9.15828	0.26319
1/16	0.32580	1.58705	9.15745	0.26318
1/32	0.32494	1.58620	9.15670	0.26319
FE method [3]				
1/4	0.36150	1.63034	9.75464	0.28351
1/8	0.32897	1.63611	9.40210	0.26703
1/16	0.32767	1.63446	9.38719	0.26633
1/32	0.32768	1.63439	9.38708	0.26632
BE method				
1/4	0.32767	1.61768	9.35607	0.26676
1/8	0.32767	1.62573	9.36930	0.26641
1/16	0.32767	1.62997	9.37778	0.26635
1/32	0.32767	1.63225	9.38214	0.26630

such that $f(p) = \phi(\tilde{z}_i)$ (see reference [4] for details). Table II clearly shows a consistent order of convergence of one. The same average p was obtained by considering other functionals and different sequences of time steps. This result is consistent with the constant discretization used in time. Table II also shows that, unlike FDM and FEM, the method is not very sensitive to Δt (this is more clearly shown in Table III); i.e., the results are as good with larger time steps as they are with smaller ones.

To further validate the numerical scheme, the problem of the collapse of a solid wall, treated in references [2, 3], is also considered for the purpose of comparison with FD and FE solutions (this will be referred to as *problem 2*). It consists of a solid wall of thickness a subjected to a constant heat flux F at $x = 0$ and thermally insulated at the extremity $x = a$ (i.e., $F_1(t) = F$ and $F_2(t) = 0$). The thermo-physical properties were taken from [3] and have the following values:

$$a = 1 \text{ m}, T(x, 0) = 27\ ^\circ\text{C}, F = 2500 \text{ W/m}^2,$$
$$C_l = C_s = 4.944 \text{ W/m}^3\ ^\circ\text{C}, K_l = K_s = 0.259 \text{ W/m}\ ^\circ\text{C},$$
$$\lambda_m = 2160 \text{ J/m}^3, \lambda_v = 37200 \text{ J/m}^3,$$
$$T_m = 1454\ ^\circ\text{C}, T_v = 3000\ ^\circ\text{C}.$$

A comparison of the time at which melting starts (t_m), the time at which vaporisation starts (t_v), the time for the collapse of the wall (t_e), and the quantity of material evaporated $V(t_e)$, respectively, for *problem 2* is shown in Table III. Table III also shows that the BEM is less sensitive to the time step size compared to FDM or FEM. However, the results shown in Table III for FDM are for variable time step,

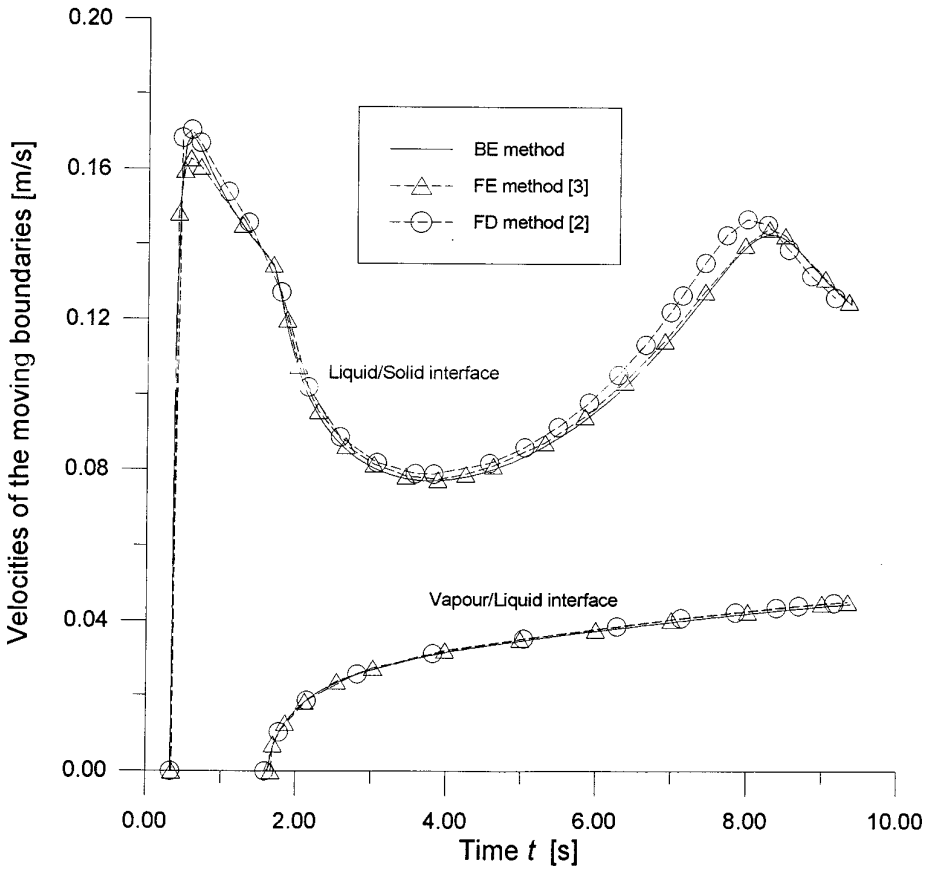

FIG. 6. Velocities versus time for *problem 2.*

but the latter remark remains valid if a constant time step is used in the FDM. Furthermore, it can be seen that the convergence of the BEM solution is much faster. For instance, there is only a difference of 4.4×10^{-4} between the computed $V(t_e)$ using the FEM with $\Delta t = 1/32$ and that of BEM with a time step 8 times larger ($\Delta t = 1/4$).

Figure 6 compares the history of the velocities of the moving boundaries, for *problem 2.* It shows that there is a good agreement between the computed velocities using the three methods. Figure 6 shows that the velocity histories of the melting and vaporisation fronts have similar behaviours as that depicted in Fig. 3. Unlike that of Fig. 3, the melting interface reaches a maximum speed just after its appearance and then starts to decrease, even before the appearance of the vapour front. This is due to a loss of temperature gradients at the interface as the melting front moves forward; however, this loss is much greater, due to the constant heat input, than that of *problem 1.* This causes the velocity of the melting front in downward trend in *problem 2*, compared to a slight decrease in the case of *problem 1.* The vaporisation front accelerates in the initial instance and then converges towards a constant velocity due to the constant heat flux input. Just before the total melting or the

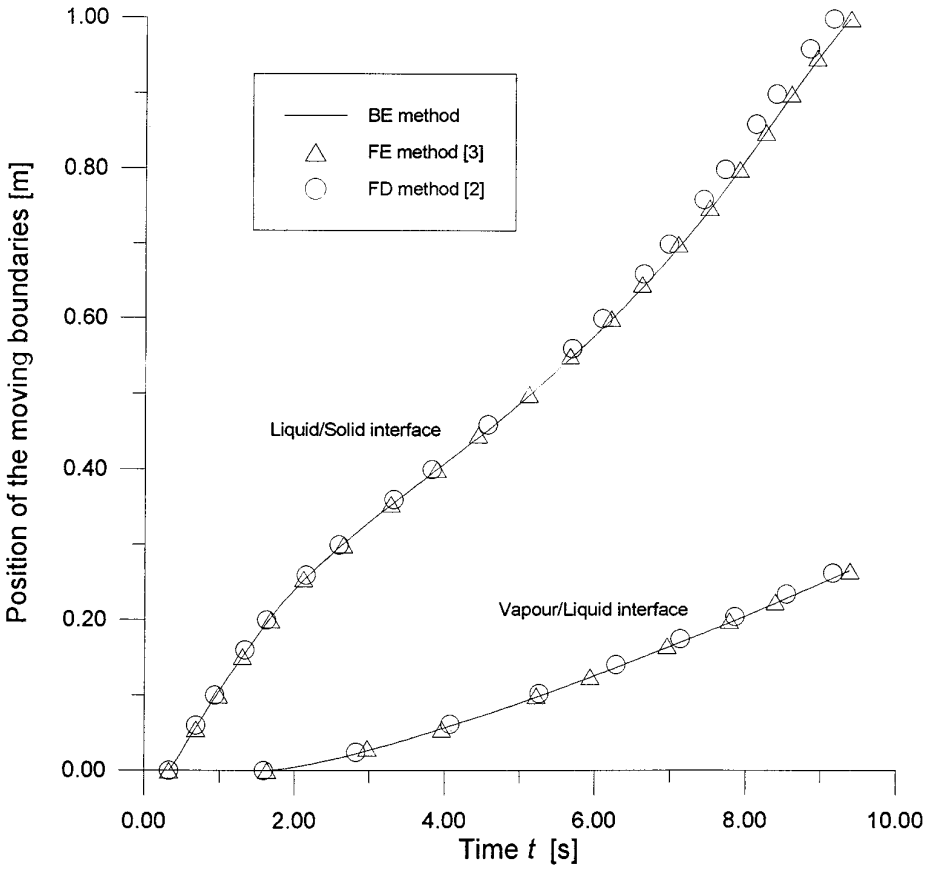

FIG. 7. Positions of the moving boundaries versus time for *problem 2.*

collapse of the wall, the melting velocity starts to decrease again due to the decreasing heat flux throughout the liquid region and the adiabatic extremity.

As with the velocities, Figs. 7 and 8 show a good agreement between the computed positions of the moving boundaries and the temperature at different positions, respectively, using the three methods. However, it must be noted that when using the FDM or FEM, the temperature inside the domain is computed at all time steps, whereas for BEM, the temperature at any position within the domain at any time can be calculated directly from the computed values and their time-history at the boundaries and the initial condition (i.e., Eq. (14) with $c(\xi) = 1$) without the need to compute its value at previous steps. In order to further validate the results, the energy balance check (i.e., Eq. (34)) is performed from the initial to the final time of the process, where the relative error between the energy provided and consumed is found to be similar to the prescribed error allowed to stop the iteration process, ϵ in Eq. (24). For example when $\epsilon = 5 \times 10^{-2}\%$, $100 \times (E_5 - \sum_{i=1}^{4} E_i)/E_5 = -5.2 \times 10^{-2}\%$, for a $\Delta t = 1/16$.

Table IV compares the solution of the system (20) with that of (25) in terms of the relative error between the two solutions (REV for velocity and REP for moving

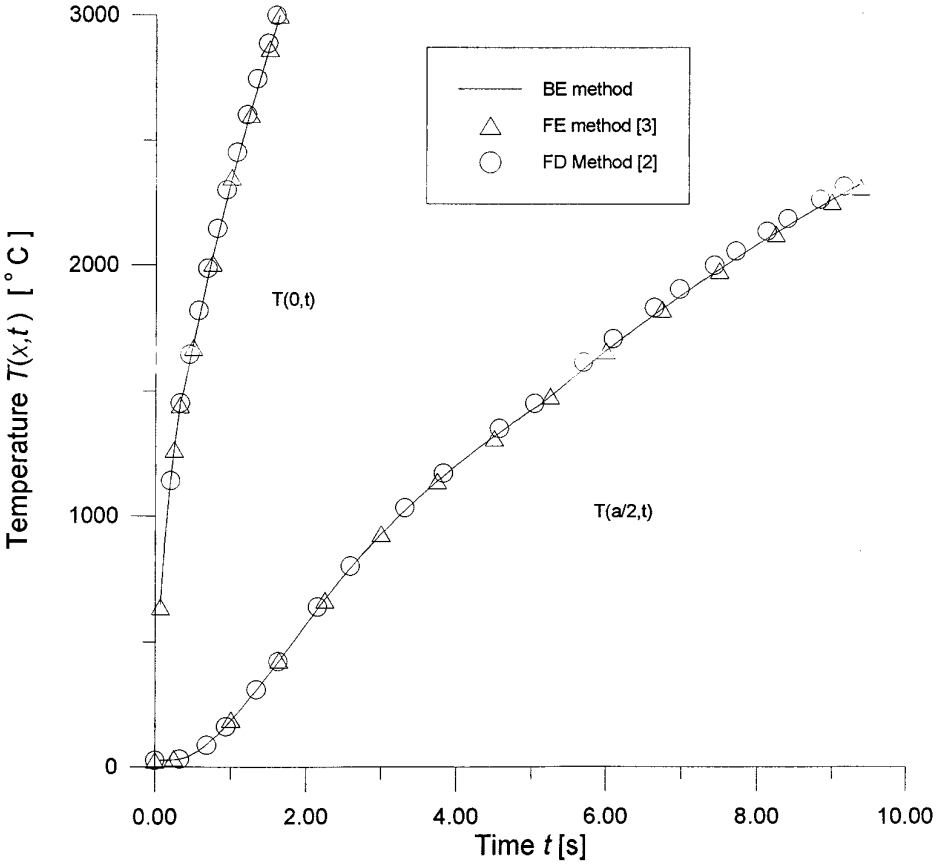

FIG. 8. Temperature at different positions versus time for *problem 2.*

boundary position), the improvement in CPU-time (CPUI), and the average number of iterations per step (AIS) for different time steps. It can be seen that the two solutions converge to each other as the time step Δt becomes smaller. However, the improvement in cpu-time decreases with Δt. This is due to the fact that the CPU-time for both solutions becomes relatively similar as the average number of iterations per step converges to one iteration.

TABLE IV
Variation of CPUI, AIS, REV, and REP with Δt

Δt	1/4	1/8	1/10	1/20	1/50
CPUI [%]	77.709	70.050	65.200	47.068	12.483
AIS	11.80	4.80	3.84	2.69	1.78
REV [%]	0.4435	0.0699	0.0364	0.0199	0.0013
REP [%]	0.1368	0.271	0.0205	0.0034	0.0021

5. CONCLUSIONS

From the numerical results shown in the previous section, it can be seen that the boundary element method is very suitable for problems with multiple moving boundaries. It can handle these problems with great ease, especially when several boundaries are simultaneously in motion. In general, refinement of the space-time mesh can be used to increase the accuracy of numerical techniques; however, this is always at the expense of greater CPU-time and memory requirements. When computations are to be performed for extended time, the use of large time steps is very desirable to reduce the computational cost. However, this results in loss of accuracy usually attendant with large meshes. Finding an optimum mesh to satisfy these paradoxes is a major problem in computational mechanics. The results show that, although the solution due to FEM and BEM are very close when the time step is small, BEM certainly outperforms its competitors when large time steps are used. This makes the BEM a more suitable choice for such problems, since it compromises between these two antagonistic concerns. Extension of the present scheme to multi-dimensional problems is straightforward from the theoretical point of view. However, evaluation of the convolution integral describing the time history of the boundary variables becomes a major task. Recent research suggests a fast algorithm capable of performing this integral in a very efficient manner, using Fourier series expansions of the Green's function [15].

APPENDIX

The integrals of the Green's function and its derivative with respect to space when the field point x is stationary are given by

$$\int_{t_1}^{t_2} G(\xi, x, t_n, t)\, dt = \frac{-r}{2\alpha\sqrt{\pi}} \left\{ \left[\frac{1}{a} \exp(-a^2) + \sqrt{\pi}\, \mathrm{erf}(a) \right]_{a_1}^{a_2} \right\}, \tag{37}$$

where

$$a_i = \frac{r}{\sqrt{4\alpha(t_n - t_i)}}, \qquad i = 1, 2 \tag{38}$$

$$\int_{t_1}^{t_2} \frac{\partial G(\xi, x, t_n, t)}{\partial x}\, dt = \frac{\mathrm{sign}(\xi - x)}{2\alpha} (\mathrm{erf}(a_2) - \mathrm{erf}(a_1)), \tag{39}$$

where $\mathrm{sign}(x) = |x|/x$ and $\mathrm{erf}(x)$ is the error function.

When the field point is moving with time, i.e., $x = X(t)$, instead of (37) and (39), the following are used:

$$\int_{t_1}^{t_2} G(\xi, X(t), t_n, t)\, dt = -\frac{1}{2v} \left\{ \exp\left(-\frac{bv}{\alpha}\right) \left[\mathrm{erf}\left(-\frac{v(t_n - t) - b}{\sqrt{4\alpha(t_n - t)}} \right) \right]_{t_1}^{t_2} + \left[\mathrm{erf}\left(-\frac{v(t_n - t) + b}{\sqrt{4\alpha(t_n - t)}} \right) \right]_{t_1}^{t_2} \right\} \tag{40}$$

for any $X(t) = x + v(t - t')$ and $b = \xi - x - v(t - t')$;

$$\int_{t_1}^{t_2} \frac{\partial G(\xi, X(t), t_n, t)}{\partial x}\, dt = -\frac{1}{2\alpha} \exp\left(-\frac{bv}{\alpha}\right)\left[\operatorname{erf}\left(-\frac{v(t_n - t) - b}{\sqrt{4\alpha(t_n - t)}}\right)\right]_{t_1}^{t_2}. \tag{41}$$

The coefficient of matrices $\mathbf{G}_j^n$ and $\mathbf{H}_j^n$ and vector $\mathbf{M}_j^n$ in Eq. (19) can be deduced from Eqs. (16) and (17) as

$$\mathbf{M}_j^n = \begin{bmatrix} \alpha_j \Psi_j^n(X_j) + \psi_j(X_j, t_n) \\ \alpha_j \Psi_j^n(X_{j+1}) + \psi_j(X_{j+1}, t_n) \end{bmatrix}, \tag{42}$$

where

$$\Psi_j^n(f) = \sum_{i=i_{j+1}}^{n-1} \left\{ g(f, X_{j+1}, t_n, t_i)\left(q_{j+1}^{i-} + \frac{1}{\alpha_j}\overline{X}_{j+1}^i u_{j+1}^i\right) - u_{j+1}^i h(f, X_{j+1}, t_n, t_i)\right\}$$
$$- \sum_{i=i_{j+1}}^{n-1} \left\{ g(f, X_j, t_n, t_i)\left(q_j^{i+} + \frac{1}{\alpha_j}\overline{X}_j^i u_j^i\right) - u_{j+1}^i h(f, X_j, t_n, t_i)\right\} \tag{43}$$

$$\mathbf{G}_j^n = \begin{bmatrix} \begin{pmatrix} \frac{1}{2} - \alpha_j h(X_j, X_j, t_n, t_n) \\ + \overline{X}_j^n g(X_j, X_j, t_n, t_n) \end{pmatrix} & \begin{pmatrix} \alpha_j h(X_j, X_{j+1}, t_n, t_n) \\ - \overline{X}_j^n g(X_j, X_{j+1}, t_n, t_n) \end{pmatrix} \\ \begin{pmatrix} -\alpha_j h(X_{j+1}, X_j, t_n, t_n) \\ + \overline{X}_j^n g(X_{j+1}, X_j, t_n, t_n) \end{pmatrix} & \begin{pmatrix} \frac{1}{2} + \alpha_j h(X_{j+1}, X_{j+1}, t_n, t_n) \\ - \overline{X}_j^n g(X_{j+1}, X_{j+1}, t_n, t_n) \end{pmatrix} \end{bmatrix} \tag{44}$$

and

$$\mathbf{H}_j^n = \alpha_j \begin{bmatrix} g(X_j, X_j, t_n, t_n) & -g(X_j, X_{j+1}, t_n, t_n) \\ g(X_{j+1}, X_j, t_n, t_n) & -g(X_{j+1}, X_{j+1}, t_n, t_n) \end{bmatrix}. \tag{45}$$

For Eq. (20), omitting the superscripts k and n, we have:

$$\mathbf{G} = \begin{bmatrix} \mathbf{G}_1 & & & \\ & \ddots & 0 & \\ & & \mathbf{G}_j & \\ & 0 & & \ddots \\ & & & \mathbf{G}_J \end{bmatrix}, \quad \mathbf{H} = \begin{bmatrix} \mathbf{H}_1 & & & \\ & \ddots & 0 & \\ & & \mathbf{H}_j & \\ & 0 & & \ddots \\ & & & \mathbf{H}_J \end{bmatrix},$$

$$\mathbf{M} = \begin{bmatrix} \mathbf{M}_1 \\ \vdots \\ \mathbf{M}_j \\ \vdots \\ \mathbf{M}_J \end{bmatrix}. \tag{46}$$

ACKNOWLEDGMENTS

This research project is supported by the Department of Trade and Industry of the United Kingdom, and forms part of the action COST-512 of the European Commission.

REFERENCES

1. J. Crank, *Free and Moving Boundary Problems* (Oxford Science Publications, Oxford, 1984), p. 163.
2. M. Zerroukat and C. R. Chatwin, A finite difference algorithm for multiple moving boundary problems using real and virtual grid networks, *J. Comput. Phys.* **112,** 298 (1994).
3. R. Bonnerot and P. Jamet, A conservative finite element method for one-dimensional Stefan problems with appearing and disappearing phases, *J. Comput. Phys.* **41,** 357 (1981).
4. R. Bonnerot and P. Jamet, A third order accurate discontinuous finite element method for the one-dimensional Stefan problem, *J. Comput. Phys.* **32,** 145 (1979).
5. C. A. Brebbia, J. C. F. Telles, and L. C. Wrobel, *Boundary Element Techniques: Theory and Application in Engineering* (Springer-Verlag, Berlin, 1984).
6. N. Zabaras and S. Mukherjee, An analysis of solidification problems by the boundary element method, *Int. J. Numer. Methods Eng.* **24,** 1879 (1987).
7. M. Erhun and S. G. Advani, A BEM approach to model heat flow during crystallization, *Int. J. Numer. Methods Eng.* **35,** 351 (1992).
8. K. O'Neill, Boundary integral equation solution of moving boundary phase change problems, *Int. J. Numer. Methods Eng.* **19,** 1825 (1983).
9. C. K. Hsieh, C. Y. Choi, and A. J. Kassab, Solution of Stefan problems by a boundary element method, in *Boundary Element Technology VII* (Computational Mechanics Publications, Southampton, and Elsevier, London, 1992), p. 473.
10. N. Zabaras, S. Mukherjee, and O. Richmond, An analysis of inverse heat transfer problems with phase changes using an integral method, *J. Heat Transfer* **110,** 554 (1988).
11. L. C. Wrobel, A boundary element solution to Stefan's problem, in *Boundary Elements V* (Computational Mechanics Publications, Southampton, and Springer-Verlag, Berlin, 1983), p. 173.
12. C. J. Coleman, A boundary integral formulation of the Stefan problem, *Appl. Math. Modelling* **10,** 445 (1986).
13. M. Heinlein, S. Mukherjee, and O. Richmond, A boundary element method analysis of temperature fields and stress during solidification, *Acta Mechanica* **59,** 59 (1986).
14. W. H. Press, S. A. Teukolsky, W. T. Vetterling, and B. P. Flannery, *Numerical Recipes in Fortran,* 2nd ed. (Cambridge Univ. Press, Cambridge, UK, 1992), p. 375.
15. L. Greengard and J. Strain, A fast algorithm for the evaluation of heat potentials, *Commun. Pure Appl. Math.* **43,** 949 (1990).